LETTER

Fermi polaron in dissipative bath with spin-orbit coupling

To cite this article: J. Zhou and W. Zhang 2021 *EPL* **134** 30004

A Letters Journal Exploring the Frontiers of Physics

May 2021

EPL, **134** (2021) 30004
doi: 10.1209/0295-5075/134/30004

www.epljournal.org

Fermi polaron in dissipative bath with spin-orbit coupling

J. Zhou[1] and W. Zhang[2,3(a)]

[1] *Department of Science, Chongqing University of Posts and Telecommunications - Chongqing 400065, China*
[2] *Department of Physics, Renmin University of China - Beijing 100872, China*
[3] *Beijing Key Laboratory of Opto-electronic Functional Materials and Micro-nano Devices, Renmin University of China - Beijing 100872, China*

received 11 December 2020; accepted in final form 12 April 2021
published online 15 July 2021

Abstract – We study the polaron problem of an impurity immersed in a dissipative spin-orbit coupled Fermi gas via a non-self-consistent T-matrix method. We first propose an experimental scheme to realize a spin-orbit coupled Fermi bath with dissipation, and show that such a system can be described by a non-Hermitian Hamiltonian that contains an imaginary spin-flip term and an imaginary constant shift term. We find that the non-Hermiticity will change the single-particle dispersion of the bath gas, and modify the properties of attractive and repulsive polarons such as energy, quasi-particle residue, effective mass, and decay rate. We also investigate the Thouless criteria corresponding to the instability of the polaron-molecule transition, which suggests a molecule state is more facilitated with stronger bath dissipation. Finally, we consider the case with finite impurity density and calculate the interaction between polarons. Our result extends the study of polaron physics to non-Hermitian systems and may be realized in future experiments.

Introduction. – Recently, the non-Hermitian system has attracted widespread attention of theorists and experimentalists. The non-Hermitian usually originates from the driven or dissipative processes induced by a bath, such as gain or loss of particle and energy from the environment. In principle, a strict approach to capture the whole characters of a driven and dissipative open system is to adopt the Lindblad equation. However, if we only consider short-time evolution where quantum jumps can be neglected, an effective non-Hermitian Hamiltonian can be approximately used to describe such systems. Non-Hermitian classical physics has been applied in many fields, for example, light propagating and scattering in a complex medium [1,2], the friction of mechanical system [3], integrating resistor in an electrical circuit [4], and biological physics [5,6].

Thanks to the recent developments in quantum technologies, non-Hermitian quantum physics plays a key role in understanding a vast number of novel phenomena in quantum open systems. One important example is the exciton-polariton system in quantum wells embedded in an optical micro-cavity. The leakage of photons from the cavity and the decay of exciton via radiative and non-radiative processes make the platform a natural quantum open system [7–9]. Ultracold quantum gases of atoms offer another highly controllable physical system to implement many non-Hermitian Hamiltonians with laser-induced one-body [10–12] and two-body [13,14] dissipation. Based on the experiment improvements, extensive theoretical works have analyzed non-Hermitian band theory [15], non-Hermitian bulk-boundary correspondence [16], non-Hermitian skin mode effect [17], topological phase transition [18], novel magnetism [19], new linear response theory [20], non-Hermitian semimetal [21,22] and dissipation-facilitated molecule [23].

The concept of polaron was originally proposed by Landau and Pekar, and further elaborated by Fröhlich and Feynman to describe the dressing effect of phonons on a Bloch electron. In contrast to an Anderson impurity, the impurity in polaron physics can move in the bath. Depending on the statistics obeyed by the bath, the polaron can be classified as Bose polaron and Fermi polaron, which have been both realized in experiment [24–34] and analyzed theoretically via various methods. For Fermi polaron, Bishop [35] used the perturbative expansion with the interaction parameter $k_F a_s$ to investigate the repulsive polaron energy. A variational approach with particle-hole excitations [36,37] is then proposed and extensively employed to treat the many-body effect in Fermi baths in different dimensionalities [38–42], with spin-orbit

(a) E-mail: wzhangl@ruc.edu.cn (corresponding author)

coupling [43], near a narrow Feshbach resonance [44,45], and for an orbital Feshbach resonance [46,47]. To further consider polaron decay, the diagrammatic many-body method is implemented to give the polaron self-energy with ladder diagram approximation [48,49]. The fixed-node quantum Monte Carlo (QMC) algorithm [50–52], the imaginary lattice quantum Monte Carlo (ILMC) [53], the functional renormalization group [54], and the non-Gaussian variational method [55] have also been adopted to analyze this topic. However, impurity in a dissipative bath has not been studied so far to the best of our knowledge.

In this work, we consider an experimentally feasible non-Hermitian Fermi bath with spin-orbit coupling, and investigate the properties of a moving impurity immersed in this dissipative background via a non-self-consistent T-matrix method and effective Hamiltonian approximation. This non-self-consistent method is proved to be equivalent to the Chevy ansatz method [36] which is used extensively to study polaron states in various configurations, and is considered to be a good approximation in the weak dissipation regime where the quasi-particle property is not drastically altered. In particular, we obtain the polaron energy of both attractive and repulsive polaron, and characterize their properties by calculating the quasi-particle residue, the effective mass, and the two-body decay rate. To connect with experiment, we calculate the detectable spectrum function of the impurity atom to show the signal variation. We also discuss the Thouless criterion [56] of pairing instability for attractive polaron branch, which suggests that a molecule state is more favorable in the strong dissipation regime. Finally, we extend our discussion to the case of finite impurity density. We calculate the variation of inter-polaron interaction energy with bath dissipation, which suggests the possibility of using dissipation as an extra controllable method in experiment. These results provide additional information about polaron physics in a dissipative bath, which is under lively investigation in various systems [57–59].

Dissipative fermi bath with spin-orbit coupling. – A dissipative spin-orbit coupled Fermi bath can be realized by a four-state scheme with three ground-state energy levels $|g_i\rangle$ and an excited state $|e\rangle$ as shown in fig. 1. Two Raman lasers Ω_1 and Ω_2 shining along the x-direction with wave vector k_0 couple $|g_1\rangle$ and $|g_2\rangle$ to the excited state $|e\rangle$, with respective detuning δ_1 and δ_2. The excited state has a large decay rate Γ to the third state $|g_3\rangle$. In order to describe the dissipative model, we introduce two Lindblad operators $S^{\pm}$ with the specific form shown in the Supplementary Material `Supplementarymaterial.pdf` (SM). Using the basis $\Phi^T = \{|g_1\rangle, |g_2\rangle, |g_3\rangle, |e\rangle\}$, the Raman coupling Hamiltonian is given by

$$H_{\text{Raman}} = \begin{pmatrix} -\delta/2 & 0 & 0 & \Omega_1^* \\ 0 & \delta/2 & 0 & \Omega_2^* \\ 0 & 0 & 0 & 0 \\ \Omega_1 & \Omega_2 & 0 & \Delta \end{pmatrix}. \tag{1}$$

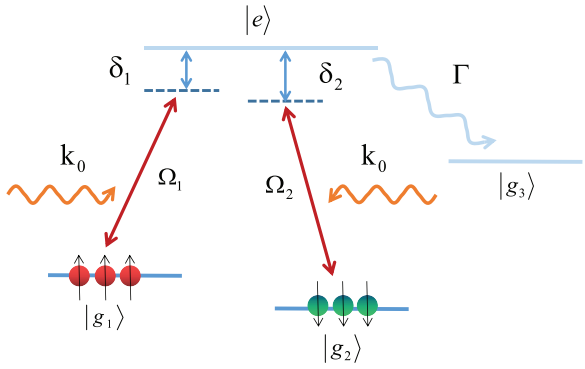

Fig. 1: Four-energy level configuration of the experimental realization of the dissipative bath with synthetic spin-orbit coupling.

Here, we define $\delta = \delta_1 - \delta_2$ and $\Delta = (\delta_1 + \delta_2)/2$ to simplify the notation. The Lindblad equation for density matrix ρ_s then takes the form

$$\frac{\mathrm{d}\rho_s}{\mathrm{d}t} = -i[H_{\text{Raman}}, \rho_s] + \Gamma\left[S^-\rho_s S^+ - \frac{1}{2}\{S^+S^-, \rho_s\}\right], \tag{2}$$

where $[\cdot,\cdot]$ and $\{\cdot,\cdot\}$ denote commutation and anti-commutation operations, respectively.

By getting the evolution of the elements of density matrix and adiabatically eliminating the excited state (details are shown in the SM), we obtain the effective Hamiltonian of the spin-orbit coupled bath

$$H_{\text{bath}}^{\text{eff}} = \frac{(\mathbf{k} + k_0\mathbf{e}_x\sigma_z)^2}{2m} - \Omega_x\sigma_x - i\Gamma_x(\sigma_x + \hat{I}). \tag{3}$$

Here, we set the Raman coupling parameters $\Omega_1 = \Omega_2 = \Omega$ to simplify the model, and use $\Omega_x = |\Omega|^2/\Delta$ and $\Gamma_x = \Gamma|\Omega|^2/\Delta^2$ to denote the spin-flip strength and single-particle dissipation, respectively. In the following discussion, we refer to the ground levels $|g_1\rangle$ and $|g_2\rangle$ as pseudo-spin $|\uparrow\rangle$ and $|\downarrow\rangle$, respectively. We further assume the interaction between the ground states $|g_i\rangle$ is negligible, and the single-particle Hamiltonian can be diagonalized to reach the energy dispersion of the background

$$\varepsilon_{\mathbf{k}\pm} = \frac{\hbar^2(\mathbf{k}^2 + k_0^2)}{2m} - i\Gamma_x \pm \sqrt{\left(\frac{\hbar^2 k_x k_0}{m}\right)^2 + (\Omega_x - i\Gamma_x)^2}. \tag{4}$$

The phase diagram of the energy dispersion is shown in fig. 2 with spin-orbit coupling parameter $(k_0/k_F)^2 = 0.5$ with k_F being the Fermi wave vector of the bath. In the following, we choose the natural unit $\hbar = m = 1$, and set the Fermi energy E_F as the energy unit. Three types of energy dispersion are observed by varying the parameters, including single-well, double-well, and triple-well structures. The triple-well type can be further divided into two sub-categories by comparing the relative depths of the central and side energy minima. In the following discussion, we fix the Raman coupling $\Omega_x = E_F$ such that the

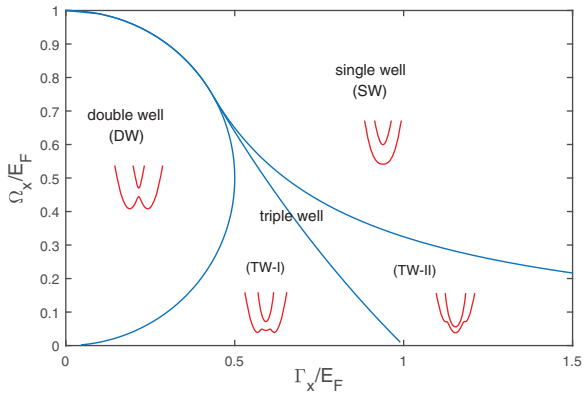

Fig. 2: Phase diagram of the single-particle dispersion. Three types of dispersion structures can by identified on this diagram, which features, respectively, a single-well (SW), a double-well (DW) and two triple-well (TW-I and TW-II) configurations. In this plot, we set $(k_0/k_F)^2 = 0.5$.

single-particle dispersion takes the single-well structure for all dissipation rates.

Then, we define the Matsubara Green's function of the bath $G^{(0)}_{\sigma\sigma'} = -\langle L|T_\tau C_{\mathbf{k}\sigma}(\tau)C^\dagger_{\mathbf{k}\sigma'}(0)|R\rangle$, where $\langle L|$ and $|R\rangle$ are the left and right eigenvectors of the non-Hermitian Hamiltonian, C and $C^\dagger$ are the fermionic operators, and T_τ is the time-ordering operator. This non-Hermitian Green's function can also be written in the following matrix form:

$$G^{(0)}(\mathbf{k}, i\omega_n) = \begin{pmatrix} G^{(0)}_{\uparrow\uparrow}(\mathbf{k}, i\omega_n) & G^{(0)}_{\uparrow\downarrow}(\mathbf{k}, i\omega_n) \\ G^{(0)}_{\downarrow\uparrow}(\mathbf{k}, i\omega_n) & G^{(0)}_{\downarrow\downarrow}(\mathbf{k}, i\omega_n) \end{pmatrix}, \tag{5}$$

where the matrix elements are given by $\mathbf{k}$,

$$\begin{aligned} G^{(0)}_{\uparrow\uparrow}(\mathbf{k}, i\omega_n) &= \frac{\psi^L_{\mathbf{k}+\uparrow}\psi^R_{\mathbf{k}+\uparrow}}{i\omega_n - \varepsilon_{\mathbf{k}+}} + \frac{\psi^L_{\mathbf{k}-\uparrow}\psi^R_{\mathbf{k}-\uparrow}}{i\omega_n - \varepsilon_{\mathbf{k}-}}, \\ G^{(0)}_{\uparrow\downarrow}(\mathbf{k}, i\omega_n) &= \frac{\psi^L_{\mathbf{k}+\uparrow}\psi^R_{\mathbf{k}+\downarrow}}{i\omega_n - \varepsilon_{\mathbf{k}+}} + \frac{\psi^L_{\mathbf{k}-\uparrow}\psi^R_{\mathbf{k}-\downarrow}}{i\omega_n - \varepsilon_{\mathbf{k}-}}, \\ G^{(0)}_{\downarrow\uparrow}(\mathbf{k}, i\omega_n) &= \frac{\psi^L_{\mathbf{k}+\downarrow}\psi^R_{\mathbf{k}+\uparrow}}{i\omega_n - \varepsilon_{\mathbf{k}+}} + \frac{\psi^L_{\mathbf{k}-\downarrow}\psi^R_{\mathbf{k}-\uparrow}}{i\omega_n - \varepsilon_{\mathbf{k}-}}, \\ G^{(0)}_{\downarrow\downarrow}(\mathbf{k}, i\omega_n) &= \frac{\psi^L_{\mathbf{k}+\downarrow}\psi^R_{\mathbf{k}+\downarrow}}{i\omega_n - \varepsilon_{\mathbf{k}+}} + \frac{\psi^L_{\mathbf{k}-\downarrow}\psi^R_{\mathbf{k}-\downarrow}}{i\omega_n - \varepsilon_{\mathbf{k}-}}. \end{aligned} \tag{6}$$

In the expressions above, $\psi^\lambda_{k\nu\sigma}$ is the transformation between the dressed-particle operator in the helix space and the original operator in the spin space, which is explained in detail in the SM.

Properties of the polaron state. – In this section, we consider a single impurity immersed in the dissipative Fermi bath with spin-orbit coupling as introduced in the previous section. The impurity is assumed to interact with one of the two ground levels (say, *e.g.*, the $|\uparrow\rangle$ state) with a tunable strength by crossing a wide Feshbach resonance. The interaction Hamiltonian takes the s-wave contact potential form

$$H_{\text{int}} = \frac{U}{V}\sum_{\mathbf{k}\mathbf{k}'\mathbf{q}} C^\dagger_{\mathbf{q}/2+\mathbf{k}\uparrow}C_{\mathbf{q}/2-\mathbf{k}'\uparrow}b^\dagger_{\mathbf{q}/2-\mathbf{k}}b_{\mathbf{q}/2+\mathbf{k}'}, \tag{7}$$

where $C_{\mathbf{k}\uparrow}$ is the annihilation operator of the spin-up fermion, $b_{\mathbf{k}}$ is the annihilation operator of the impurity, and V is the quantization volume. We then use the many-body T-matrix theory to solve for the self-energy of the impurity. By keeping all the ladder-type diagrams, the self-energy at temperature T is given as

$$\Sigma_{\text{tot}}(\mathbf{k}, i\omega_n) = k_B T \sum_{\mathbf{q}, i\Omega_n} G^{(0)}_{\uparrow\uparrow}(\mathbf{q}-\mathbf{k}, i\Omega_n - i\omega_n)\Gamma(\mathbf{q}, i\Omega_n), \tag{8}$$

where the vertex function Γ can be written through the Bethe-Slapeter equation as

$$\begin{aligned} \Gamma(\mathbf{q}, i\Omega_n)^{-1} &= \frac{1}{U} \\ &+ k_B T \sum_{\mathbf{k}, i\omega} G^{(0)}(\mathbf{k}, i\omega)G^{(0)}_{\uparrow\uparrow}(\mathbf{q}-\mathbf{k}, i\Omega_n - i\omega). \end{aligned} \tag{9}$$

Here, the free Green's function of the impurity takes the form $G^{(0)}(\mathbf{k}, i\omega) = 1/(i\omega - \epsilon^I_{\mathbf{k}})$ with impurity dispersion $\epsilon^I_{\mathbf{k}}$. Note that the vertex function has two parts which are contributed by the two helicity bands of the spin-orbit coupled Fermi background.

At zero temperature, after summing up the Matsubara frequency, the retarded self-energy is given by

$$\begin{aligned} \Sigma^R_{\text{tot}}(\mathbf{k}, i\Omega_n) = \frac{1}{V}\sum_{\mathbf{q}} \big[&\Theta(-\varepsilon_{\mathbf{q}+})\Phi_{+\uparrow}\Gamma^R(\mathbf{q}+\mathbf{k}, \varepsilon_{\mathbf{q}+} + \omega^+) \\ &+\Theta(-\varepsilon_{\mathbf{q}-})\Phi_{-\uparrow}\Gamma^R(\mathbf{q}+\mathbf{k}, \varepsilon_{\mathbf{q}-} + \omega^+)\big]. \end{aligned} \tag{10}$$

Here, $\Phi_{+\uparrow} = \psi^L_{\mathbf{q}+\uparrow}\psi^R_{\mathbf{q}+\uparrow}$, $\Phi_{-\uparrow} = \psi^L_{\mathbf{q}-\uparrow}\psi^R_{\mathbf{q}-\uparrow}$, and $\Theta(x)$ is the Heaviside step function as the zero-temperature limit of the Fermi-Dirac function. Owing to the non-Hermiticity of the spin-orbit coupled bath, there is an imaginary part in the dispersion $\varepsilon_{\mathbf{k}\pm}$. However, we only consider the real part of the dispersion energy in the step function, because the imaginary part is connected with the life time of the dressed particle and only shows oscillation behaviors in the distribution function. We adopt a non-self-consistent "G_0G_0" theory in the calculation which has been proved equivalent to the variational wave function approach [36].

Once the self-energy is obtained, we can get the quasi-particle properties of the impurity from the retarded impurity Green's function

$$G^R_I(\mathbf{k}, \omega^+) = \frac{1}{\omega - (\epsilon_{\mathbf{k}} - \mu_I) - \Sigma^R_{\text{tot}}(\mathbf{k}, \omega + i\eta^+) + i\eta^+}, \tag{11}$$

where $\epsilon_{\mathbf{k}}$ is the impurity dispersion, and μ_I is the corresponding chemical potential. In fact, within the quasi-particle approximation, the retarded impurity Green's

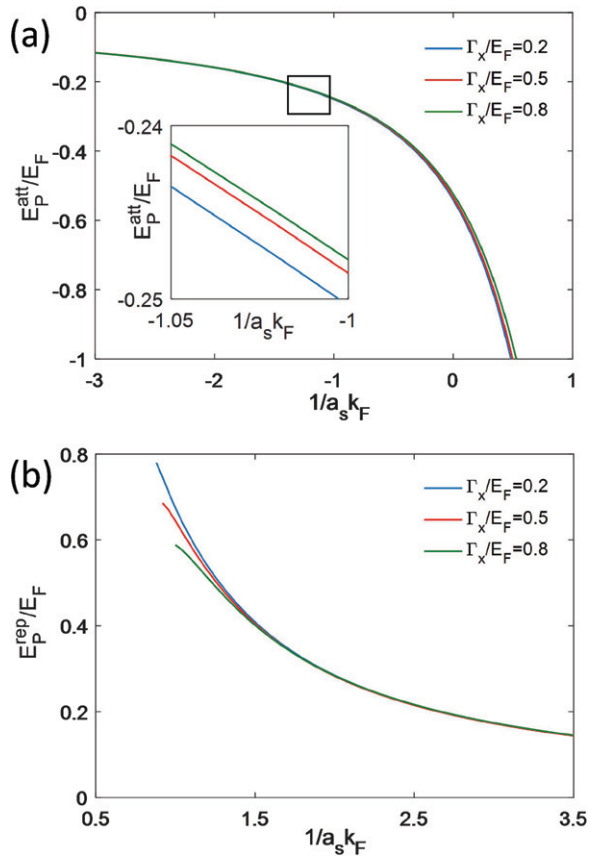

Fig. 3: Polaron energy of the (a) attractive branch $E_P^{\rm att}$ and (b) repulsive branch $E_P^{\rm rep}$. Lines in all panels are plotted with $\Gamma_x/E_F = 0.2$ (blue), 0.5 (red), and 0.8 (green). We choose $(k_0/k_F)^2 = 0.5$ and $\Omega_x/E_F = 1$.

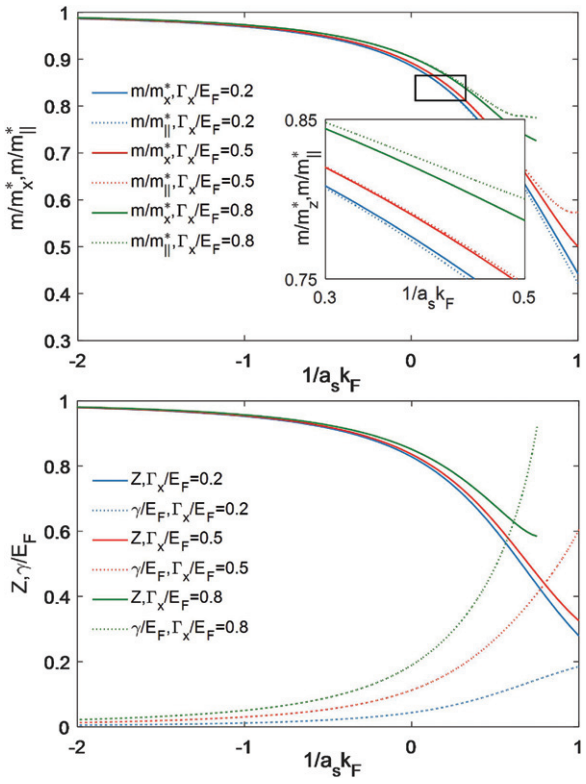

Fig. 4: (a) Effective mass along the k_x (solid) and $k_{||}$ (dotted) directions of the attractive polaron state. (b) Quasi-particle residue (solid) and two-body decay rate (dotted) of the attractive polaron state. Lines in all panels are plotted with $\Gamma_x/E_F = 0.2$ (blue), 0.5 (red), and 0.8 (green). Parameters are chosen to be same as in fig. 3.

function can also be expressed with quasi-particle ratio Z, effective mass $m^*_{\rm eff}$ and two-body decay rate γ. Considering the symmetry of the dispersion of the spin-orbit coupled bath, the dressed impurity would have two effective masses m_x^* and $m_y^* = m_z^* = m_{||}^*$. Thus, in the low-energy and long-wavelength limit, the retarded impurity Green's function takes the form

$$G_I^R(\mathbf{k},\omega^+) = \frac{Z}{\omega - \hbar^2 k_{||}^2/2m_{||}^* - \hbar^2 k_x^2/2m_x^* + \mu_I - E_P + i\gamma/2}, \quad (12)$$

where $k_{||}^2 = k_y^2 + k_z^2$. Compared with the two forms of retarded Green's functions, the energy of the polaron state can be determined as

$$E_P = {\rm Re}\Sigma^R_{\rm tot}(\mathbf{k}=0, E_P - \mu_I), \quad (13)$$

and the quasi-particle properties are characterized by

$$Z = \frac{1}{1 - \frac{\partial {\rm Re}\Sigma^R_{\rm tot}}{\partial\omega}}, \quad (14)$$

$$\frac{m}{m_{||}^*} = \frac{1 + \frac{\partial {\rm Re}\Sigma_{\rm tot}}{\partial\epsilon_{||}}}{1 - \frac{\partial {\rm Re}\Sigma^R_{\rm tot}}{\partial\omega}}, \quad (15)$$

$$\frac{m}{m_x^*} = \frac{1 + \frac{\partial {\rm Re}\Sigma^R_{\rm tot}}{\partial\epsilon_x}}{1 - \frac{\partial {\rm Re}\Sigma^R_{tot}}{\partial\omega}}, \quad (16)$$

$$\gamma = -2Z{\rm Im}\Sigma^R_{\rm tot}, \quad (17)$$

In the expressions above, $\epsilon_{||}$ and ϵ_x are impurity dispersions along $k_{||}$ and k_x, respectively.

In fig. 3 and fig. 4, we show the energy, effective mass, quasi-particle residue, and two-body decay rate for polaron states with different bath dissipation strength. As depicted in figs. 3(a) and (b), the polaron energy increases with dissipation strength for the attractive polaron branch and decreases for the repulsive branch. The dependence is negligible in the deep Bardeen-Cooper-Schrieffer (BCS) limit for the attractive branch, and also in the Bose-Einstein condensate (BEC) limit for the repulsive branch, but becomes sizable around the unitary region. Owing to the presence of the one-dimensional spin-orbit coupling, the effective mass of the attractive polaron state acquires an anisotropy with different m_x^* and $m_{||}^*$, as shown in fig. 4(a). The two effective masses both increase monotonically by crossing the Feshbach resonance from the BCS side to the BEC side, implying that the dressing effect is more significant on the impurity by the background with

increasing interaction. On the other hand, the dissipation tends to make the impurity less inert and reduce the effective masses in all directions. An interesting finding is that for small dissipation, the polaron is easier to move along the x-direction with $m_x^* < m_{||}^*$. But the anisotropy inverses with increasing dissipation, showing a subtle competition between dissipation and anisotropic energy dispersion induced by spin-orbit coupling.

In fig. 4(b), we plot the quasi-particle residue and two-body decay rate of the attractive polaron state. Notice that the impurity acquires larger quasi-particle residue with increasing dissipation, indicating that the impurity behaves more like an independent particle in that regime. This observation is qualitatively consistent with the trends shown in figs. 3(a) and 4(a). Finally, although the impurity does not have a direct decay channel, a larger bath dissipation will induce more severe decay of the attractive polaron state. This increase of the polaron decay rate is a direct result of the elevation of both the quasi-particle residue Z and the imaginary part of retarded Green's function. Physically, it can be qualitatively understood by noticing that when the damping magnitude Γ_x is increased, the Fermi surface of the background would be deformed to be more anisotropic, such that the surface area and density of states are both enhanced. However, we emphasize that our results are only restricted to weak dissipation systems, where the non-self-consisitent method we employed is considered to be valid. Another interesting finding is that the decay rate γ is sensitively dependent on the damping magnitude Γ_x on the strongly interacting BEC regime, hence can be used as an experimental indicator to reveal the effect induced by the lossy background via radio-frequency spectroscopy [60].

Next, we investigate the polaron-molecule transition. Owing to the strong attractive interaction in the BEC regime, the impurity atom will be tightly bounded with the bath fermion to form a dimer state. Such a transition point can be well described by the Thouless criterion of pairing instability $\Gamma^{-1}(\mathbf{q}=0, i\Omega_n=0)=0$ for a non-dissipative Fermi system. However, in the present configuration of a dissipative bath, the Thouless criterion cannot be fully satisfied due to the presence of an imaginary part in the vertex function. Thus, we show in fig. 5(a) only the real part of $\Gamma^{-1}(\mathbf{q}=0, i\Omega_n=0)$, and neglect its imaginary part. We find that a larger bath dissipation tends to push the polaron-molecule transition point from the deep BEC limit towards the unitarity region, implying that the molecule state is more favorable with stronger dissipation.

To make a direct connection with experiments, we show in fig. 5(b) the spectrum function which can be detected by spectroscopic measurement. Two peaks are observed and can be attributed respectively to the attractive and repulsive polaron states. By increasing the dissipative strength from $\Gamma_x/E_F = 0.2$ to $\Gamma_x/E_F = 0.8$ with scattering length $1/a_s k_F = 0.5$ and SOC strength $(k_0/k_F)^2 = 0.5$, both peaks are shifted according to the results of figs. 3(a) and (b), and are significantly extended with smaller intensity owing to the stronger decay.

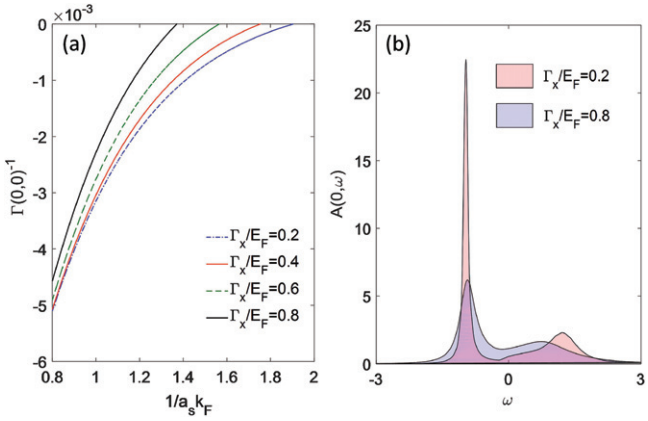

Fig. 5: (a) The Thouless criteria of the pairing instability for different dissipative strength. In this scheme, the polaron-molecule transition takes place at the point where $\Gamma(0,0)^{-1}$ reaches zero. (b) Spectrum function with different bath dissipation for $1/a_s k_F = 0.5$. Other parameters are chosen to be same as in fig. 3.

Interaction between attractive polarons. – In this section, we consider the case of a finite impurity density to calculate the interaction between attractive polarons. Since the normal state of a highly imbalanced Fermi mixture can be understood as a Fermi liquid at zero temperature [61], the ground-state energy of this three components Fermi gases can be written in the form of the Landau-Pomeranchuk law as a function of the impurity concentration $x = n_{\rm imp}/n_{\rm bath}$,

$$E = E_{\rm bath} + f(E_b)x + g(m_{||}^*/m, m_x^*/m)x^{5/3} + Fx^2, \qquad (18)$$

where $E_{\rm bath}$ is the kinetic energy of the non-interacting spin-orbit coupled bath. The second term comes from the binding energy of the impurity quasi-particles in the background Fermi sea, the third term corresponds to the kinetic energy of the impurity atoms, and the last term is defined as the energy arising from the polaron-polaron interaction. The coefficient F of the last term thus labels the interaction intensity which can be obtained by a numerical fitting of the total energy.

With the Gibbs-Duhem relation $\partial P/\partial\mu_B = n_{\rm bath}$ and $\partial P/\partial\mu_I = n_{\rm imp}$, we can obtain the grand-canonical equation of state

$$P = \int_{\min(E_{k-})}^{\mu_B} n_{\rm bath}(\mu)\mathrm{d}\mu + \int_0^{\mu_I} n_{\rm imp}(\mu)\mathrm{d}\mu. \qquad (19)$$

Here, P is the pressure of the system, $\min(E_{k-})$ is the lowest energy band of the dissipative spin-orbit coupled bath, and μ_B and μ_I are the chemical potentials of the bath and the impurity, respectively. We need to emphasize that μ_B and μ_I are not the bare chemical potentials (Fermi energies) but include the contribution from the interaction.

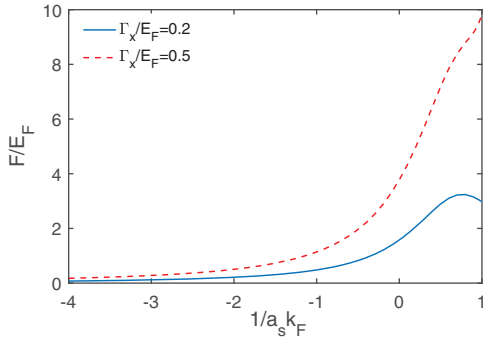

Fig. 6: Polaron-polaron interaction parameter F *vs.* scattering length with different dissipation strengths. Parameters are chosen to be same as in fig. 3.

In order to get the total energy of the system, we convert the equation of state to the canonical ensemble, and get the relations of chemical potentials

$$n_{\rm bath}(\mu_B) = n_{\rm bath}\left(1 + x\frac{\partial E_P}{\partial \mu_B}\Big|_{\mu_B = E_{BF}}\right), \tag{20}$$

$$\mu_I = E_P + E_{IF}. \tag{21}$$

Here, $E_{BF} = \hbar^2 k_{BF}^2/2m$ and $E_{IF} = \hbar^2 k_{IF}^2/2m$. From the first relation, we can have the renormalized bath chemical potential from the bare one (see the SM for details). The second relation means that one has to cost a polaron energy E_P plus an impurity Fermi energy E_{IF} to add an impurity atom to the system with finite impurity concentration. Then, we arrive at the canonical ensemble energy function,

$$E = -\sum_{i=B,I} P_i V_i + \sum_{i=B,I} \mu_i N_i. \tag{22}$$

Rearranging the total energy E in different powers of x and fitting the coefficient of the x^2 term, we can get the polaron-polaron interacting parameter F *vs.* scattering length with different dissipative strength Γ_x. As illustrated in fig. 6, if the dissipative strength is small ($\Gamma_x/E_F = 0.2$), the parameter F increases first and then decreases by crossing the Feshbach resonance from the BCS to the BEC sides. However, if the dissipation is large enough, *e.g.*, $\Gamma_x/E_F = 0.5$, F keeps increasing in the parameter region of scattering length considered here. We also note that the polaron-polaron interaction is enhanced by the dissipation within the entire parameter range shown in fig. 6. This observation can be attributed to the following two reasons. First, the quasi-particle residue is increased with dissipation as depicted in fig. 4(b), and hence contribute positively to the interaction strength [59]. In addition, the dissipative term of Γ_x induces anisotropy into the Fermi background, which leads to a deformed effective Fermi surface with a larger surface area and enhanced density of states. The polaron-polaron interaction can also be calculated by a combined theory of Landau Fermi liquid and microscopic self-consistent method, which can also be applied to the repulsive branch. However, owing to the anisotropy induced by the spin-orbit coupling, this method is very costly in numerics as discussed in the SM.

Conclusion and outlook. – In conclusion, we propose an experimentally feasible realization of a non-Hermitian spin-orbit coupled bath. Based on the effective Hamiltonian of the bath gases, we use non-self-consistent T-matrix theory to solve the polaron problem in the weak dissipation regime. We obtain the variation of the polaron energy and quasi-particle parameters with different bath dissipation strength. Furthermore, we use Landau-Pomeranchuk energy to describe the system energy in the low impurity concentration [61], and investigate the polaron-polaron interaction for different scattering lengths and bath dissipations.

We also notice that Wasak *et al.* have used the Keldysh Green's function method to solve the dissipative polaron and molecule states in the absence of spin-orbit coupling [62]. However, in our system, there is no direct dissipation for the impurity. The dissipation bath, therefore, provides a complex self-energy to the impurity atom, which is similar to the finite temperature polaron or the repulsive polaron states. So, we can omit the jump terms in the Lindblad equation, and use an effective non-Hermitian Hamiltonian and many-body T-matrix [48] to solve the polaron problem.

* * *

We acknowledge Wei Yi, Hui Hu, Jia Wang, Ran Qi, Xiaoling Cui, Lihong Zhou, Wei Zheng, and JiaZhen Sun for helpful discussion. This work is supported by the National Natural Science Foundation of China (Grants No. 11504038, No. 11522436, No. 11774425), the National Key R&D Program of China (Grant No. 2018YFA0306501), the Beijing Natural Science Foundation (Z180013), the Joint fund of the Ministry of Education (6141A020333xx), and the Research Funds of Renmin University of China (Grants No. 16XNLQ03 and No. 18XNLQ15).

REFERENCES

[1] Beenakker C. W. J., *Rev. Mod. Phys.*, **69** (1997) 731.
[2] Makris K. G., El-Ganainy R., Christodoulides D. N. and Musslimani Z. H., *Phys. Rev. Lett.*, **100** (2008) 103904.
[3] Susstrunk R. and Huber S. D., *Proc. Natl. Acad. Sci. U.S.A.*, **113** (2016) E4767.
[4] Schindler J., Li A., Zheng M. C., Ellis F. M. and Kottos T., *Phys. Rev. A*, **84** (2011) 040101(R).
[5] Celardo G. L., Borgonovi F., Merkli M., Tsifrinovich V. I. and Berman G. P., *J. Phys. Chem. C*, **116** (2012) 22105.
[6] Celardo G. L., Giusteri G. G. and Borgonovi F., *Phys. Rev. B*, **90** (2014) 075113.

[7] Deng H., Weihs G., Santori C., Bloch J. and Yamamoto Y., *Science*, **298** (2002) 199.
[8] Kasprzak J. *et al.*, *Nature*, **443** (2006) 409.
[9] Balili R., Hartwell V., Snoke D., Pfeiffer L. and West K., *Science*, **316** (2007) 1007.
[10] Li J., Harter A. K., Liu J., de Melo L., Joglekar Y. N. and Luo L., *Nat. Commun.*, **10** (2019) 855.
[11] Lapp S., Angóngá J., Alex An F. and Gadway B., *New. J. Phys.*, **21** (2019) 045006.
[12] Bouganne R., Aguilera M. B., Ghermaoui A., Beugnon J. and Gerbier F., *Nat. Phys.*, **16** (2020) 21.
[13] Tomita T., Nakajima S., Danshita I., Takasu Y. and Takahashi Y., *Sci. Adv.*, **3** (2017) e1701513.
[14] Tomita T., Nakajima S., Takasu Y. and Takahashi Y., *Phys. Rev. A*, **99** (2019) 031601(R).
[15] Yokomizo K. and Murakami S., *Phys. Rev. Lett.*, **123** (2019) 066404.
[16] Yang Z., Zhang K., Fang C. and Hu J., *Phys. Rev. Lett.*, **125** (2020) 226402.
[17] Yi Y. and Yang Z., *Phys. Rev. Lett.*, **125** (2020) 186802.
[18] Hou J., Wu Y.-J. and Zhang C., arXiv:1910.14606 (2019).
[19] Zhang X. Z., Jin L. and Song Z., arXiv:2006.01324 (2020).
[20] Pan L., Chen X., Chen Y. and Zhai H., *Nat. Phys.*, **16** (2020) 767.
[21] Kawabata K., Bessho T. and Sato M., *Phys. Rev. Lett.*, **123** (2019) 066405.
[22] Yang Z., Chiu C.-K., Fang C. and Hu J., *Phys. Rev. Lett.*, **124** (2020) 186402.
[23] Zhou L., Yi W. and Cui X., *Phys. Rev. A*, **102** (2020) 043310.
[24] Chikkatur A. P., Görlitz A., Stamper-Kurn D. M., Inouye S., Gupta S. and Ketterle W., *Phys. Rev. Lett.*, **85** (2000) 483.
[25] Catani J., Lamporesi G., Naik D., Gring M., Inguscio M., Minardi F., Kantian A. and Giamarchi T., *Phys. Rev. A*, **85** (2012) 023623.
[26] Spethmann N., Kindermann F., John S., Weber C., Meschede D. and Widera A., *Phys. Rev. Lett.*, **109** (2012) 235301.
[27] Scelle R., Rentrop T., Trautmann A., Schuster T. and Oberthaler M. K., *Phys. Rev. Lett.*, **111** (2013) 070401.
[28] Schirotzek A., Wu C.-H., Sommer A. and Zwierlein M. W., *Phys. Rev. Lett.*, **102** (2009) 230402.
[29] Kohstall C., Zaccanti M., Jag M., Trenkwalder A., Massignan P., Bruun G. M., Schreck F. and Grimm R., *Nature*, **485** (2012) 615.
[30] Koschorreck M., Pertot D., Vogt E., Fröhlich B., Feld M. and Köhl M., *Nature*, **485** (2012) 619.
[31] Jorgensen N. B., Wacker L., Skalmstang K. T., Parish M. M., Levinsen J., Christensen R. S., Bruun G. M. and Arlt J. J., *Phys. Rev. Lett.*, **117** (2016) 055302.
[32] Hu M.-G., Van de Graaff M. J., Kedar D., Corson J. P., Cornell E. A. and Jin D. S., *Phys. Rev. Lett.*, **117** (2016) 055301.
[33] Yan Z. Z., Ni Y., Robens C. and Zwierlein M. W., arXiv:1904.02685 (2019).
[34] Skou M. G., Skov T. G., Jørgensen N. B., Nielsen K. K., Camacho-Guardian A., Pohl T., Bruun G. M. and Arlt J. J., *Nat. Phys.*, **17** (2021) 731.
[35] Bishop R. F., *Ann. Phys.*, **78** (1973) 391.
[36] Chevy F., *Phys. Rev. A*, **74** (2006) 063628.
[37] Cui X. and Zhai H., *Phys. Rev. A*, **81** (2010) 041602(R).
[38] Zöllner S., Bruun G. M. and Pethick C. J., *Phys. Rev. A*, **83** (2011) 021603(R).
[39] Parish M. M., *Phys. Rev. A*, **83** (2011) 051603(R).
[40] Parish M. M. and Levinsen J., *Phys. Rev. A*, **87** (2013) 033616.
[41] Doggen E. V. H., Korolyuk A., Törmä P. and Kinnunen J. J., *Phys. Rev. A*, **89** (2014) 053621.
[42] Kwasniok J., Mistakidis S. I. and Schmelcher P., *Phys. Rev. A*, **101** (2020) 053619.
[43] Yi W. and Zhang W., *Phys. Rev. Lett.*, **109** (2012) 140402.
[44] Massignan P., *EPL*, **98** (2012) 10012.
[45] Qi R. and Zhai H., *Phys. Rev. A*, **85** (2012) 041603(R).
[46] Chen J.-G., Deng T.-S., Yi W. and Zhang W., *Phys. Rev. A*, **94** (2016) 053627.
[47] Deng T.-S., Lu Z.-C., Shi Y.-R., Chen J.-G., Zhang W. and Yi W., *Phys. Rev. A*, **97** (2018) 013635.
[48] Combescot R., Recati A., Lobo C. and Chevy F., *Phys. Rev. Lett.*, **98** (2007) 180402.
[49] Massignan P. and Bruun G. M., *Eur. Phys. J. D*, **65** (2011) 83.
[50] Prokofév N. V. and Svistunov B. V., *Phys. Rev. B*, **77** (2008) 020408(R).
[51] Prokofév N. V. and Svistunov B. V., *Phys. Rev. B*, **77** (2008) 125101.
[52] Vlietinck J., Ryckebusch J. and Van Houcke K., *Phys. Rev. B*, **87** (2013) 115133.
[53] Bour S., Lee D., Hammer H.-W. and Meissner Ulf-G., *Phys. Rev. Lett.*, **115** (2015) 185301.
[54] Schmidt R. and Enss T., *Phys. Rev.*, **83** (2011) 063620.
[55] Liu R., Shi Y.-R. and Zhang W., *Phys. Rev. A*, **102** (2020) 033305.
[56] Nozieres P. and Schmitt-Rink S., *J. Low Temp. Phys.*, **59** (1985) 195.
[57] Tan L. B., Cotlet O., Bergschneider A., Schmidt R., Back P., Shimazaki Y., Kroner M. and Imamoglu A., *Phys. Rev. X*, **10** (2020) 021011.
[58] Emmanuele R. P. A. *et al.*, *Nat. Commun.*, **11** (2020) 3589.
[59] Bastarrachea-Magnani M. A., Camacho-Guardian A. and Bruun G. M., arXiv:2008.10303 (2020).
[60] Scazza F., Valtolina G., Massignan P., Recati A., Amico A., Burchianti A., Fort C., Inguscio M., Zaccanti M. and Roati G., *Phys. Rev. Lett.*, **118** (2017) 083602.
[61] Mora C. and Chevy F., *Phys. Rev. Lett.*, **104** (2010) 230402.
[62] Wasak T., Schmidt R. and Piazza F., arXiv:1912.06618 (2019).